Proceedings of the ASME 2016 International Mechanical Engineering Congress and Exposition
IMECE2016
November 11-17, 2016, Phoenix, Arizona, USA

IMECE2016-65876

MICROMECHANICS MODELLING OF GRAPHENE PLATELETS REINFORCED POLYMER COMPOSITE MATERIALS WITH IMPERFECT INTERFACES

Wiyao Leleng Azoti
Faculty of Applied Sciences
Department of Computing, Engineering and Technology
University of Sunderland, SR6 0DD, UK

Ahmed Elmarakbi
Faculty of Applied Sciences
Department of Computing, Engineering and Technology
University of Sunderland, SR6 0DD, UK

ABSTRACT

This work investigates the elasto-plastic response of platelets-like inclusions reinforced polymer composites showing an imperfect interface. The solution of the heterogeneous material problem is solved through a kinematic integral equation. To account for the interfacial behaviour, a linear spring model LSM is adopted, leading to an expression of the modified Eshelby's tensor. As a consequence, the interfacial contributions with respect to the strain concentration tensor within each phase as well as in the average strain field are described by a modified version of the Mori-Tanaka scheme for the overall response. The non-linear response is established in the framework of the J_2 flow rule. An expression of the algorithmic tangent operator for each phase can be obtained and used as uniform modulus for homogenisation purpose. Numerical results are conducted on graphene platelets GPL-reinforced polymer PA6 composite for several design parameters such as GPL volume fraction, aspect ratio and the interfacial compliance. These results clearly highlight the impact of the aspect ratio as well as the volume fraction by a softening in the overall response when imperfection is considered at the interface. Present developments are analytical-based solutions. They constitute a theoretical framework for further multi-scale applications in automotive. The crashworthiness simulation incorporating an influence of the interfacial behaviour on the strain energy absorption SEA is of interest.

Keywords: Interface, Modified Eshelby's tensor, Micromechanics, Graphene platelets.

1 INTRODUCTION

The enhancement of nano composites properties has gained worthy significance with use of multifunctional nano fillers like the graphene. This latter finds direct applications with polymer composite materials where substantial property enhancements have been noticed at much lower volume fraction [1] with respect to polymer composites containing conventional micron-scale fillers (such as glass or carbon fibres). For deriving such properties, multi scale analyses combining molecular mechanics theories and continuum models have been developed for graphene polymer composites. The graphene properties are often derived at atomistic scale and the nano particles are treated as equivalent continuum particles [2, 3] that are embedded in the polymer matrix through conventional homogenisation techniques.

Despite graphene has been used to increase stiffness, toughness and thermal conductivity of polymer resins by a large margin [4, 5, 6, 7], there are still much technological challenges to overcome mainly in the material modelling. This is characterised by the lack of sufficient knowledge on graphene composites for structural applications describing interfacial properties between graphene and polymer matrix under severe loading conditions. It is well-known that the interface characterises the load transfer between the particles/fibres and the matrix. Therefore, it represents an influential parameter that can significantly change the overall properties. Indeed, interface is subjected to defects (debonding, dislocations and cracks) between reinforcements and the matrix and can be identified as one of the predominant damage mechanics in particle and fibre-reinforced composites [8]. Then, the accuracy of the composite response needs a proper accounting for the properties of the interface. Several micromechanics models have been developed for that purpose. Among them, one can distinguish the interphase models as well as interface models. The firsts i.e the interphase models

Copyright © 2016 by ASME

introduce the interfacial zone as a layer (with a given thickness and properties) between the particle or fibres and the matrix. First interphase model known as "three-phase model" are due to Walpole [9] and then followed by works by Christensen and Lo [10], Herve and Zaoui [11], Cherkaoui et al. [12] and Lipinski et al. [13]. The seconds i.e the interface models introduce discontinuities in the displacement and/or stress fields at the interface. One can refer to cohesive zone models CZM (Matous and Guebelle [14], Inglis et al. [15], Tan et al. [16, 17]), free sliding model FSM (Ghahremani [18]) and interface stress model ISM (Sharma et al. [19], Sharma and Ganti [20], Sharma and Wheeler [21], Duan et al. [22, 23]) as well as linear spring model LSM (Hashin [24, 25], Qu [26, 27], Zhong and Meguid [28]). Other models for instance the dislocation-like approach in works by Yu et al. [29, 30] and finally the equivalent inclusion concept in works by Zhao and Weng [31, 32] which later have been used by Yanase and Ju [8] to study the damage response of spherical particles reinforced composites, should be cited.

This work aims to analyse the effect of an imperfect interface on the non-linear response of graphene platelets GPL composite materials. The properties of the GPL which have been widely derived at atomistic scale are not the scope of this work. Herein, advantage is taken of these derivations by considering GPL as continuum phases interacting with the polymer matrix through a slightly weakened interface. The LSM model is then considered for its simplicity and flexibility to treat imperfect interface with limited number of model parameters [8]. The solution of the heterogeneous material problem is obtained by the kinematic integral equation of Dederichs and Zeller [33]. The non-linear framework, which is that recently used by Azoti et al. [34, 35], is based on a Hill-type incremental formulation and the classical J_2 flow rule. Therefore, for each phase, the consistent (algorithmic) tangent operator is obtained from the continuum (elasto-plastic) tangent operator and thus from works by Doghri and Ouaar [36]. By accounting for the contribution of the interface, on the one hand inside the strain concentration tensor of the inclusions through the modified Eshelby tensor [26, 27], and on the other hand in the average strain field, a modified version of the Mori-Tanaka is derived for the effective properties.

The paper is organised as follows: section 2 establishes the general framework of a multi-scale homogenisation by deriving the global strain concentration tensor; in section 3, the algorithmic tangent operators derived from the classical J_2 flow theory are recalled. Section 4 gives expressions of the imperfect interface in terms of traction and displacements as well as the modified Eshelby's tensor while section 5 derives the modified Mori-Tanaka scheme for overall responses. The model predictions are therefore compared with open literature data in section 6 where a systematic analysis of micro parameters (aspect ratio, volume fraction, interfacial compliance) is carried out for a GPL-reinforced polymer PA6 under uniaxial tests.

2 FUNDAMENTALS OF MICROMECHANICS

2.1 Kinematic integral equation

Let us consider a composite material consisting of $N+1$ phases. The matrix (phase 0) can be a specific constituent containing all remaining phases. To study this composite, a representative volume element (RVE) is considered. On the RVE boundaries (Fig. 1), admissible macroscopic static or kinematic loads are applied in the absence of body forces and inertia terms. The micromechanics scale transition consists, firstly, in the localisation of the macroscopic strain tensor $\mathbf{E}$ through a fourth order global strain concentration tensor $\mathbf{A}(r)$ and, secondly, in the homogenisation, which uses averaging techniques to approximate the macroscopic behaviour. Note that $\mathbf{A}(r)$ remains the unknown parameter that contains all the information about the microstructure. The effective properties of the RVE are given by:

$$\mathbf{C}^{eff} = \frac{1}{V}\int_V \boldsymbol{c}(r) : \mathbf{A}(r) dV \tag{1}$$

where $\boldsymbol{c}(r)$ denotes the local uniform modulus and V the volume of the RVE. The operator ":" stands for the tensorial contraction over two indices. The global strain concentration tensor $\mathbf{A}(r)$ links the local strain $\boldsymbol{\varepsilon}(r)$ to the macroscopic strain $\mathbf{E}$ as follows:

$$\boldsymbol{\varepsilon}(r) = \mathbf{A}(r) : \mathbf{E} \tag{2}$$

The decomposition of the local uniform modulus into a homogeneous reference part $\boldsymbol{c}^R$ and a fluctuation part $\delta\boldsymbol{c}$ is given such as:

$$\boldsymbol{c}(r) = \boldsymbol{c}^R(r) + \delta\boldsymbol{c}(r) \tag{3}$$

Equation (3) enables the derivation of the kinematic integral equation of Dederichs and Zeller [33]. In terms of strain fields, the kinematic integral equation reads:

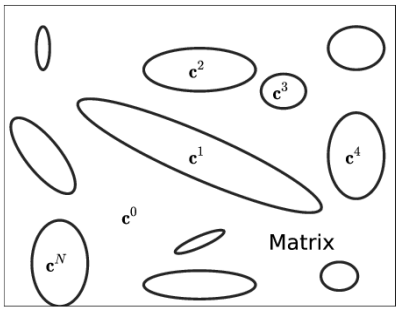

Figure 1. Illustration of a RVE

$$\boldsymbol{\varepsilon}(r) = \mathbf{E}^R - \int_V \boldsymbol{\Gamma}(r-r') \delta\boldsymbol{c}(r') \boldsymbol{\varepsilon}(r') dV' \tag{4}$$

Copyright © 2016 by ASME

where $\mathbf{E}^R$ is the strain field inside the reference infinite medium and $\boldsymbol{\Gamma}(r-r')$ is the modified Green tensor.

2.2 Global strain concentration tensor based on Eshelby's ellipsoidal inclusion

The kinematic integral equation (4) represents the formal solution the global strain concentration tensor is derived from. Based on an iterative procedure proposed by Vieville et al. [37], the global strain concentration tensor $\mathbf{A}^I(r)$ for a I^{th} phase of the RVE is given as:

$$\begin{cases} \mathbf{A}^I(r) = \boldsymbol{a}^I(r) : \left[\overline{\boldsymbol{a}}^I(r)\right]^{-1} \\ \overline{\mathbf{A}}^I(r) = \mathbf{I} \end{cases} \tag{5}$$

$\mathbf{I}$ represents the fourth order symmetric identity tensor and $\overline{\bullet}$ is the mean-field volume average of $\bullet$. The quantity $\boldsymbol{a}^I(r)$ is the local strain concentration tensor with respect to the reference medium such that:

$$\boldsymbol{\varepsilon}^I(r) = \boldsymbol{a}^I(r) : \mathbf{E}^R \tag{6}$$

The I^{th} concentration tensor $\boldsymbol{a}^I(r)$ is given by:

$$\begin{cases} \boldsymbol{a}^I{}_0(r) = \mathbf{I} \\ \boldsymbol{a}^I{}_{i+1}(r) = \left[\mathbf{I} + \boldsymbol{T}^{II} : \Delta\boldsymbol{c}^I(r)\right]^{-1} \\ \qquad\qquad : \left(\mathbf{I} - \sum_{\substack{J=0 \\ J\neq I}}^{N} \boldsymbol{T}^{IJ} : \Delta\boldsymbol{c}^J(r) : \boldsymbol{a}^J{}_i(r) \right) \\ I = 0,1,2,3,.....,N \end{cases} \tag{7}$$

with N the number of phases considered in the composite. $\Delta\boldsymbol{c}^I(r) = \boldsymbol{c}^I(r) - \boldsymbol{c}^R(r)$. In equation (7), $\boldsymbol{a}^I{}_i(r)$ represents an approximation of the I^{th} concentration tensor at iteration i. $\boldsymbol{T}^{II}$ and $\boldsymbol{T}^{IJ}$ are the interaction tensors in one-site (OS) and multi-site (MS) versions, respectively. Their general expression is:

$$\boldsymbol{T}^{IJ} = \frac{1}{V_I} \int_{V_I} \int_{V_J} \boldsymbol{\Gamma}(r-r') dV dV' \tag{8}$$

The computational framework of $\boldsymbol{T}^{II}$ and $\boldsymbol{T}^{IJ}$ is proposed by Fassi-Fehri [38].

Let us suppose that the geometry of any phase within the RVE is ellipsoidal. The Eshelby's inclusion concept [39] assumes that the strain field inside an ellipsoidal inclusion is uniform. Therefore, a characteristic function $\theta(r)$ can be defined such as [37]:

$$\theta(r) = \begin{cases} 1 \text{ if } r \in V_I \\ 0 \text{ if } r \notin V \end{cases} \tag{9}$$

Based on equation (9) and the average strain field within an inclusion I such as:

$$\boldsymbol{\varepsilon}^I = \frac{1}{V_I} \int_{V_I} \boldsymbol{\varepsilon}(r) dV \tag{10}$$

the above kinematic integral Eq. (4) can be rewritten as:

$$\begin{cases} \boldsymbol{\varepsilon}^I = \mathbf{E}^R - \sum_{J=0}^{N} \boldsymbol{T}^{IJ} : \Delta\boldsymbol{c}^J : \boldsymbol{\varepsilon}^J \\ I = 0,1,2,3,.....,N \end{cases} \tag{11}$$

and the local concentration tensor Eq. (7) becomes:

$$\begin{cases} \boldsymbol{a}^I{}_0 = \mathbf{I} \\ \boldsymbol{a}^I{}_{i+1} = \left[\mathbf{I} + \boldsymbol{T}^{II} : \Delta\boldsymbol{c}^I\right]^{-1} \\ \qquad\qquad : \left(\mathbf{I} - \sum_{\substack{J=0 \\ J\neq I}}^{N} \boldsymbol{T}^{IJ} : \Delta\boldsymbol{c}^J : \boldsymbol{a}^J{}_i \right) \\ I = 0,1,2,3,.....,N \end{cases} \tag{12}$$

In the case of OS version (most frequent developments in the literature) and for isotropic medium, the interaction tensor $\boldsymbol{T}^{II}$ can be deduced from the Eshelby's tensor $\mathbf{S}$ such as $\boldsymbol{T}^{II} = \mathbf{S} : \left(\boldsymbol{c}^R\right)^{-1}$ In such condition and neglecting the interactions among inclusion I and its neighbours J, i.e. all the tensors $\boldsymbol{T}^{IJ} = 0$, the local concentration tensor $\boldsymbol{a}^I$ reads more simple expression:

$$\begin{cases} \boldsymbol{a}^I = \left[\mathbf{I} + \mathbf{S} : \left(\boldsymbol{c}^R\right)^{-1} : \Delta\boldsymbol{c}^I\right]^{-1} \\ I = 0,1,2,3,.....,N \end{cases} \tag{13}$$

Finally, the global strain concentration tensor $\mathbf{A}^I$ is calculated by substituting Eq. (13) in Eq. (5) Therefore, for any homogenization model defined by $\mathbf{A}^I$, the effective or macro-stiffness tensor $\mathbf{C}^{eff}$ is given through a discrete form of the Eq. (1) by:

$$\mathbf{C}^{eff} = \sum_{I=0}^{N} f_I \boldsymbol{c}^I : \mathbf{A}^I \tag{14}$$

with the volume fraction f_I defined as:

$$f_I = \frac{V_I}{V} \tag{15}$$

3 NON LINEAR TANGENT OPERATORS

Let us consider that one or more phases behave elasto-plastically within the RVE. Referring to the work of Doghri and Ouaar [36], at least two tangent operators can be defined: the "continuum" (or elasto-plastic) $\mathbf{C}^{ep}$ tangent operator, which is derived from the rate constitutive equation, and the "consistent" (or algorithmic) $\mathbf{C}^{alg}$ tangent operator, which is solved from a discretisation of the rate equation in time interval $[t_n, t_{n+1}]$:

$$\begin{cases} \dot{\boldsymbol{\sigma}} = \mathbf{C}^{ep} : \dot{\boldsymbol{\varepsilon}} \\ \delta\boldsymbol{\sigma}_{n+1} = \mathbf{C}^{alg} : \delta\boldsymbol{\varepsilon}_{n+1} \end{cases} \tag{16}$$

The explicit expressions of the tangent operators are derived from the classical J_2 flow rule such as:

Copyright © 2016 by ASME

$$\begin{cases} \mathbf{C}^{ep} = \mathbf{C}^{el} - \dfrac{(2G)^2}{h}\mathbf{N}\otimes\mathbf{N} \\ h = 3G + \dfrac{dR}{dp} > 0 \end{cases} \tag{17}$$

$$\begin{cases} \mathbf{C}^{alg} = \mathbf{C}^{ep} - (2G)^2 \Delta p \dfrac{\sigma_{eq}}{\sigma_{eq}^{tr}} \dfrac{\partial \mathbf{N}}{\partial \boldsymbol{\sigma}} \\ \dfrac{\partial \mathbf{N}}{\partial \boldsymbol{\sigma}} = \dfrac{1}{\sigma_{eq}}\left(\dfrac{3}{2}\mathbf{I}_{dev} - \mathbf{N}\otimes\mathbf{N}\right) \end{cases} \tag{18}$$

In equations (17) and (18), G denotes the material shear modulus while the operator "⊗" designates the tensorial product. $\mathbf{C}^{el}$ represents the elastic stiffness tensor and $R(p)$ is the hardening stress with p the accumulated plastic strain. $\mathbf{N}$ represents the normal to the yield surface in the stress space. σ_{eq}^{tr} denotes a trial elastic predictor of σ_{eq}. $\mathbf{I}_{dev}$ stands for the deviatoric part of the fourth order symmetric identity tensor. The knowledge of internal variables such as Δp and σ_{eq}^{tr} remains crucial for computation of the algorithmic tangent operator $\mathbf{C}^{alg}$ in Eq. (18). This tangent operator will be later used as uniform modulus to compute the overall behaviour of the composite in section 5. A detailed procedure about internal variables computation can be found in [35].

4 IMPERFECT INTERFACE AND THE MODIFIED ESHELBY'S TENSOR

Let us consider the interface γ between two phases of a composite material. The linear spring model LSM supposes the continuity of the traction vector across the interface while the jump of displacement field is considered to be proportional to the traction on that interface. These assumptions are written like:

$$\begin{cases} \Delta\sigma_{ij} n_j = \left[\sigma_{ij}\left(\gamma^+\right) - \sigma_{ij}\left(\gamma^-\right)\right] n_j = 0 \\ \Delta u_i = \left[u_i\left(\gamma^+\right) - u_i\left(\gamma^-\right)\right] = \eta_{ij}\sigma_{jk} n_k \end{cases} \tag{19}$$

with n_j the components of a unit vector normal to the interface. $u_i\left(\gamma^+\right)$ and $u_i\left(\gamma^-\right)$ stand for the values of $u_i(x)$ when x reaches the interface from outside and inside of the inclusion respectively. $\sigma_{ij}\left(\gamma^+\right)$ and $\sigma_{ij}\left(\gamma^-\right)$ are the dual in terms of stress. The second order tensor components η_{ij} denote the compliance of the interface. It appears that $\eta_{ij} = 0$ leads to a perfectly bonded interface whereas $\eta_{ij} \to \infty$ represents a completely debonded interface. The expression of η_{ij} is given by [26, 27]:

$$\eta_{ij} = \alpha\delta_{ij} + (\beta - \alpha) n_i n_j \tag{20}$$

where the constants α and β stand for the extent of interfacial sliding and the interfacial separation, respectively. δ_{ij} is the Kronecker symbol. In the case of ellipsoidal inclusions, Qu [26, 27] has determined the Eshelby's tensor for these inclusions embedded in an elastic matrix and showing a slightly weakened interface i.e when η_{ij} is very small. Therefore, the modified Eshelby's tensor for this problem yields:

$$\mathbf{S}^{\mathbf{M}} = \mathbf{S} + (\mathbf{I} - \mathbf{S}) : \mathbf{H} : \boldsymbol{c} : (\mathbf{I} - \mathbf{S}) \tag{21}$$

where $\mathbf{S}$ denotes the original Eshelby's tensor [39] and $\mathbf{H}$ stands for a four order tensor depending on the interface properties and the geometry of the inclusion. Expressions of $\mathbf{H}$ for ellipsoidal inclusions are given in Appendix. In others terms, Eq. (21) can be written such as:

$$\begin{aligned} S_{ijkl}^{\mathbf{M}} &= S_{ijkl} + \left(I_{ijpq} - S_{ijpq}\right) H_{pqrs} \\ &\quad \times C_{rsmn}\left(I_{mnkl} - S_{mnkl}\right) \end{aligned} \tag{22}$$

5 MODIFIED MORI-TANAKA SCHEME FOR OVERALL RESPONSES

General considerations on Mori-Tanaka scheme can be found in works by Azoti et al. [34]. Therefore, the MT effective properties are given by:

$$\begin{cases} \mathbf{C}^{MT} = \displaystyle\sum_{I=0}^{N} f_I \boldsymbol{c}^I : \mathbf{A}^I \\ \qquad = \left(f_0 \boldsymbol{c}^0 + \displaystyle\sum_{I=1}^{N} f_I \boldsymbol{c}^I : \boldsymbol{a}^I \right) : \mathbf{A}^0 \end{cases} \tag{23}$$

with $\mathbf{A}^0$ the global strain concentration of the matrix. By accounting for the interface contributions, modifications come out with the definition of the average strain field:

$$\begin{cases} \mathbf{E} = \dfrac{1}{V}\displaystyle\int_V \boldsymbol{\varepsilon}(x) dV \\ \qquad = \displaystyle\sum_{I=0}^{N} f_I \boldsymbol{\varepsilon}^I + \dfrac{1}{V}\int_{\gamma} \dfrac{1}{2}\left(\Delta\mathbf{u}\otimes\mathbf{n} + \mathbf{n}\otimes\Delta\mathbf{u}\right) dS \end{cases} \tag{24}$$

where γ represents the union of all interfaces. The combination of Eq.(19)-b and Eq.(24) leads to the following expression of the average strain:

$$\begin{cases} \mathbf{E} = \displaystyle\sum_{I=0}^{N} f_I \boldsymbol{\varepsilon}^I \\ \qquad + \dfrac{1}{V}\displaystyle\sum_{I=1}^{N} \int_{\gamma_I} \dfrac{1}{2}\left[\left(\boldsymbol{\eta}.\boldsymbol{\sigma}.\mathbf{n}\right)\otimes\mathbf{n} + \mathbf{n}\otimes\left(\boldsymbol{\eta}.\boldsymbol{\sigma}.\mathbf{n}\right)\right] dS \end{cases} \tag{25}$$

with γ_I the surface of the volume V_I.

The evaluation of the integral terms in Eq.(25) remains tricky for an arbitrary interface geometry. However by taking advantage of developments by Qu [26] for slightly weakened

Copyright © 2016 by ASME

interface, the stress distribution on the surface γ_I can be replaced by its average over the volume V_I leading to a simplified form of Eq.(25) such as:

$$\mathbf{E} = \sum_{I=0}^{N} f_I \boldsymbol{\varepsilon}^I + \sum_{I=1}^{N} f_I \mathbf{H}^I : \boldsymbol{\sigma}^I \tag{26}$$

Using Eq.(5) and derivations in works [34], one can demonstrate the following relationship between the average strain within an inclusion and the matrix such as:

$$\boldsymbol{\varepsilon}^I = \boldsymbol{a}^I : \boldsymbol{\varepsilon}^0 \tag{27}$$

where $\boldsymbol{a}^I$ in the OS-version yields:

$$\begin{cases} \boldsymbol{a}^I = \left[\mathbf{I} + \mathbf{S}^{\mathbf{M}} : \left(\boldsymbol{c}^R \right)^{-1} : \Delta \boldsymbol{c}^I \right]^{-1} \\ I = 1, 2, 3, ..., N \end{cases} \tag{28}$$

Combining Eq.(27) and Eq.(26) leads to

$$\mathbf{E} = \left[\sum_{I=0}^{N} f_I \boldsymbol{a}^I + \sum_{I=1}^{N} f_I \mathbf{H}^I : \boldsymbol{c}^I : \boldsymbol{a}^I \right] : \boldsymbol{\varepsilon}^0 \tag{29}$$

The inversion of Eq.(29)

$$\boldsymbol{\varepsilon}^0 = \left[\sum_{I=0}^{N} f_I \boldsymbol{a}^I + \sum_{I=1}^{N} f_I \mathbf{H}^I : \boldsymbol{c}^I : \boldsymbol{a}^I \right]^{-1} : \mathbf{E} \tag{30}$$

in conjunction with Eq.(2) leads to the modified global concentration tensor of the matrix $\mathbf{A}^0$ such as:

$$\mathbf{A}^0 = \left[\sum_{I=0}^{N} f_I \boldsymbol{a}^I + \sum_{I=1}^{N} f_I \mathbf{H}^I : \boldsymbol{c}^I : \boldsymbol{a}^I \right]^{-1} \tag{31}$$

Substituting Eq.(31) into Eq.(23) gives the modified Mori-Tanaka effective properties such as:

$$\begin{cases} \mathbf{C}^{MT}_{\mathrm{mod}ified} = \left(f_0 \boldsymbol{c}^0 + \sum_{I=1}^{N} f_I \boldsymbol{c}^I : \boldsymbol{a}^I \right) \\ \qquad : \left[\sum_{I=0}^{N} f_I \boldsymbol{a}^I + \sum_{I=1}^{N} f_I \mathbf{H}^I : \boldsymbol{c}^I : \boldsymbol{a}^I \right]^{-1} \end{cases} \tag{32}$$

In the case a 2-phase composite, Eq.(32) yields

$$\begin{cases} \mathbf{C}^{MT}_{\mathrm{mod}ified} = \left(f_0 \boldsymbol{c}^0 + f_I \boldsymbol{c}^I : \boldsymbol{a}^I \right) \\ \qquad : \left[f_0 \mathbf{I} + f_I \left(\mathbf{I} + \mathbf{H}^I : \boldsymbol{c}^I \right) : \boldsymbol{a}^I \right]^{-1} \end{cases} \tag{33}$$

6 NUMERICAL RESULTS AND DISCUSSIONS

6.1 Model validations

The capability of the present model to reproduce results from the open literature is carried out herein. In a first instance, the model predictions are compared with the earlier works by Qu [26]. Let us consider a composite consisting of an isotropic matrix and aligned isotropic ellipsoidal inclusions of dimensions (a_1, a_2, a_3) with aspect ratio AR such as $AR = a_3/a_1$ and $a_1 = a_2 = a$. A pure sliding case is considered i.e $\alpha \neq 0$ and $\beta = 0$. The sliding interfacial separation constant α is given such as $\alpha = a\alpha_0/\mu_0$ with α_0 the sliding coefficient and a the ellipsoid semi-axis. The material properties for this analysis are gathered in Table 1.

Table 1. Material properties from works by Qu [26]

Matrix		Inclusions				
μ_0	ν_0	μ_I	ν_I	AR	α	β
1.0GPa	0.4	30GPa	0.25	2.0	$a\alpha_0/\mu_0$	0

Table 2. Material properties from works by Yanase and Ju [8]

Matrix		Inclusions			
E_0	ν_0	E_I	ν_I	AR	β
3.0GPa	0.4	76.0GPa	0.23	1.0	0

Figure 2 shows the evolution of the normalised effective transverse and longitudinal Young modulus E_{11}/μ_0 and E_{33}/μ_0 as well as the effective longitudinal Poisson's ratio ν_{31} versus the volume fraction of the inclusions. These predictions are concerned with the originate Mori-Tanaka scheme for perfect bonded inclusions denoted MT, the originate MT using only the modified Eshelby's tensor denoted MT, $\alpha_0 = 0.3$, and finally the modified MT using the modified Eshelby's tensor denoted $Modif.MT$, $\alpha_0 = 0.3$. Different trends are obtained for the Young moduli and the Poisson's ratio. Indeed, the higher the inclusions volume fraction, the higher the Young moduli E_{11}/μ_0 and E_{33}/μ_0. However, accounting for a pure sliding interface has led to a decrease of the effective stiffness. For the Poisson's ratio ν_{31}, while a decrease is noticed for others methods i.e MT and MT, $\alpha_0 = 0.3$, a parabolic trend is observed when a weakened interface $Modif.MT$, $\alpha_0 = 0.3$ is accounting for with a minimum at $f_I = 0.3$. A fair agreement is found between the present predictions with respect to results by Qu [26] showing by the way the effectiveness of the numerical integration method used for solving equations in the Appendix.

Furthermore, the present model is confronted to results by Yanase and Ju [8] on spherical particle-reinforced composites. The material properties used for this study is presented in Table 2.

Figure 3 presents the influence of the sliding coefficient α_0 on the normalised effective Young modulus E_{eff}/E_0. Under the perfect interface condition, i.e $\alpha_0 = 0$ and beyond a volume fraction $f_I = 0.2$ the MT scheme underestimates results by Yanase and Ju [8]. One can explain this observation by the well-known accuracy issues with the MT when a high volume fraction is achieved. Subsequently, when the interface

Copyright © 2016 by ASME

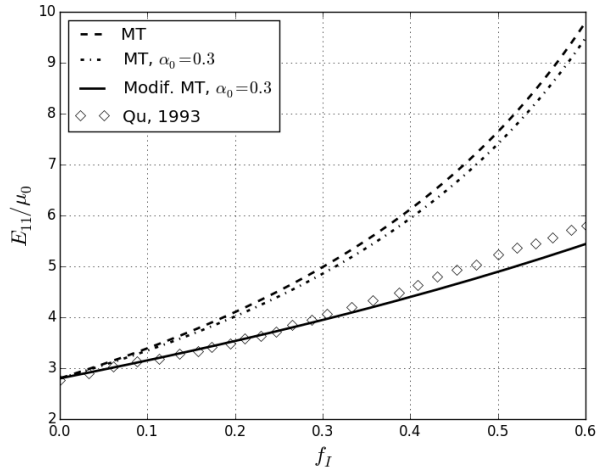

(a) E_{11}/μ_0

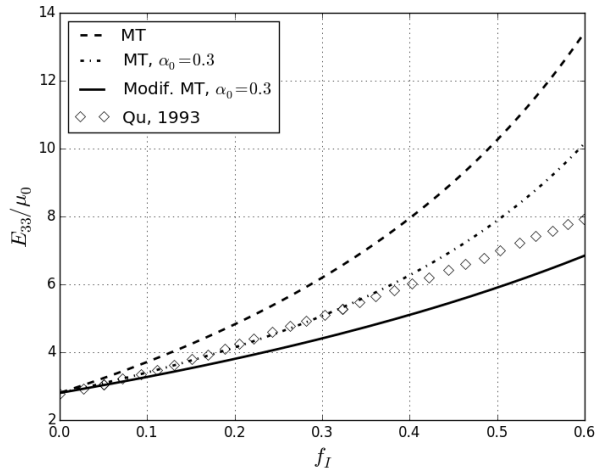

(b) E_{33}/μ_0

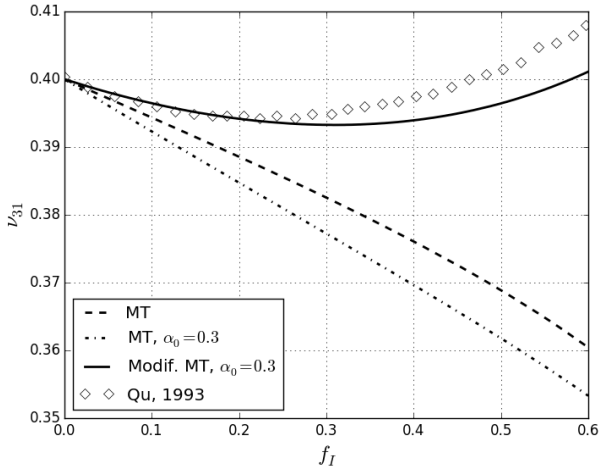

(c) ν_{31}

Figure 2. Effective elastic moduli of ellipsoidal inclusions reinforced composite

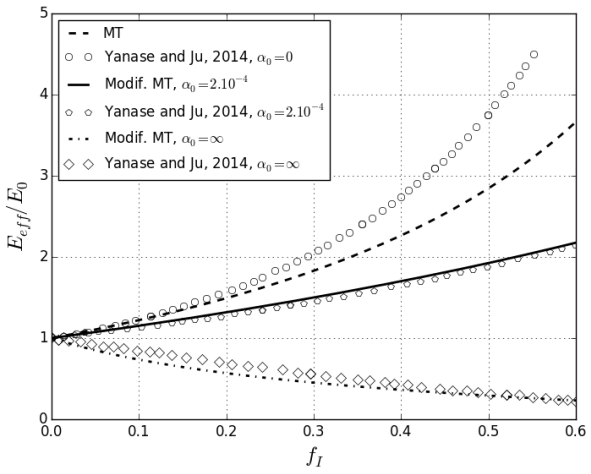

Figure 3. Effective young modulus of spherical particles reinforced composite

imperfection is considered with $\alpha_0 = 2.10^{-4}$, a significant decrease of the E_{eff}/E_0 is noticed with respect to the case of perfect interface. However, the effective response shows an increase with the volume fraction and good agreement is obtained with results by Yanase and Ju [8]. For high interface damage i.e $\alpha_0 = \infty$, E_{eff}/E_0 shows a decrease with the volume fraction evolution. Again, the predictions remain in good agreement with results by Yanase and Ju [8].

Table 3. Material properties for GPL/PA-6 composite materials

Matrix					Inclusions	
E_0	ν_0	σ_Y	h	m	E_I	ν_I
2GPa	0.39	60.5MPa	63MPa	0.4	10^3GPa	0.22

6.2 GPL-reinforced polymer PA-6 composite materials

As application of the present development to polymer composite, a GPL reinforced PA-6 polymer matrix is considered. The GPL are assumed elastic while the PA-6 matrix is considered elasto-plastic with an isotropic hardening power law defined as $R(r) = hr^m$. The material properties are presented in Table 3. The macro stress-strain response is studied under uniaxial loading. The loading is given by a macro stain increment $\Delta\mathbf{E} = \Delta E\, \boldsymbol{\psi}$ with $\boldsymbol{\psi} = \mathbf{e}_1 \otimes \mathbf{e}_1 - \frac{1}{2}\left[\mathbf{e}_2 \otimes \mathbf{e}_2 + \mathbf{e}_3 \otimes \mathbf{e}_3\right]$. The effective response of the composite is assessed through different design parameters for instance the platelets aspect ratio AR, the volume fraction f_I and the interface sliding coefficient α_0.

Copyright © 2016 by ASME

Figure 4 shows the evolution of the equivalent stress-strain response versus the AR. This parameter has a significant impact on the effective response. Indeed, an increase of the effective stiffness is noticed with the decrease of the AR. Lower values such as $AR = 10^{-1}$ corresponding to platelets-like shape show more effective reinforcement character than circular-like shape i.e $AR = 1$.

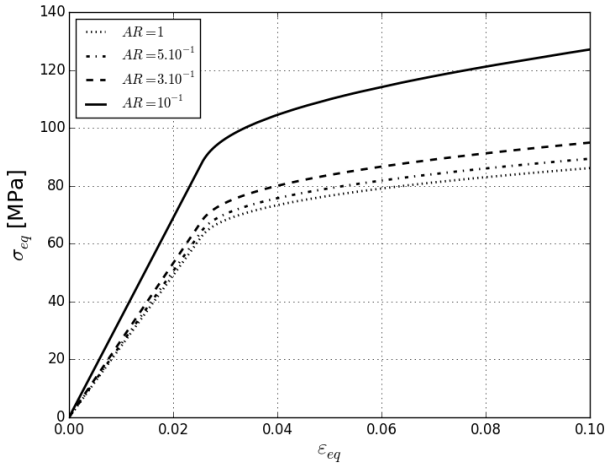

Figure 4. Aspect ratio variation of GPL/PA-6 composite for $f_I = 0.1$ and $\alpha_0 = 0.3$

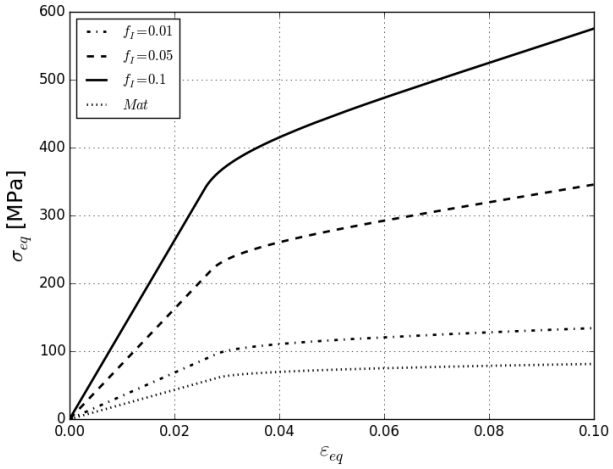

Figure 5. Volume fraction variation of GPL/PA-6 composite for $AR = 10^{-2}$ and $\alpha_0 = 0.3$

In addition, the variation of the volume fraction f_I is analysed in Figure 5. The predictions reproduce a trend similar to the matrix for $f_I = 0$ and subsequently shifts towards higher stress with the increase of f_I. The influence of the interface imperfection is analysed in Figures 6 and 7. The higher the sliding coefficient α_0, the lower and softer the effective stress-strain response as shown by Figure 6. In Figure 7, the results obtained from a perfect interface and an imperfect interface modelling are compared. the higher the volume fraction, the higher the gap between the two responses and the lower the effective response that accounts for the interface imperfection.

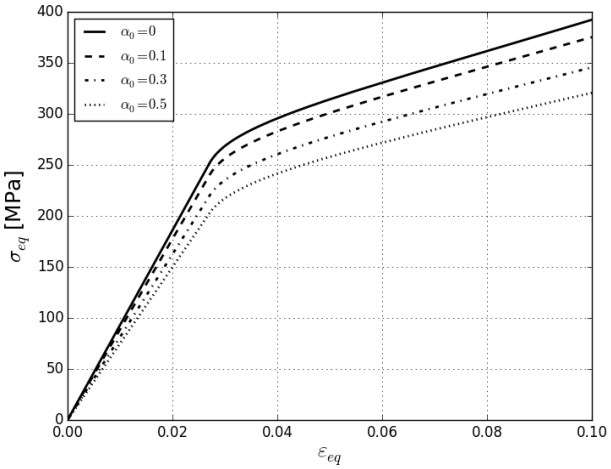

Figure 6. Interface sliding compliance variation of GPL/PA-6 composite for $AR = 10^{-2}$

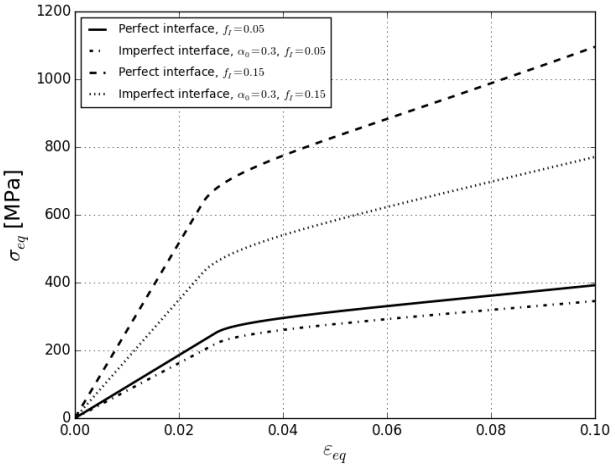

Figure 7. Influence of imperfect versus perfect interface of GPL/PA-6 composite for $AR = 10^{-2}$

6 CONCLUSION

The nonlinear elasto-plastic response of graphene platelets reinforced PA-6 polymer has been analysed regarding the interfacial behaviour. For such a purpose, the linear spring model LSM is considered for its simplicity and flexibility to treat imperfection at the interface with limited number of model parameters. Therefore, a modified expression is obtained for both the Eshelby's tensor and the Mori-Tanaka scheme for deriving the effective response of the composite.

Results highlight the importance of the aspect ratio that leads to the most effective reinforcement response at low values. By considering imperfection, the sliding coefficient also shows a significant impact on the composite response versus the volume fraction. The higher the volume fraction, the higher the softening in the stress-stress response.

Copyright © 2016 by ASME

The present developments are purely analytical-based heterogeneous composites solutions. They are therefore less computationally expensive than FE analysis. Results of this study are expected to be integrated in the design of new graphene based composite for automotive applications. As perspective, the influence of the sliding coefficient α_0 in a multi-scale crashworthiness simulation is of interest mainly for the determination of the strain energy absorption SEA. This micromechanics solution can therefore be related to each Gauss integration point within the macro-model.

ACKNOWLEDGMENTS

The research leading to these results has received funding from the European Union Seventh Framework Programme under grant agreement No. **604391 Graphene Flagship**

APPENDIX

The components of the interfacial tensor $\mathbf{H}$ are given by:

$$H_{ijkl} = \alpha P_{ijkl} + (\beta - \alpha) Q_{ijkl} \tag{34}$$

where P_{ijkl} and Q_{ijkl} are given for ellipsoidal inclusions by:

$$\begin{cases} P_{ijkl} = \dfrac{3}{16\pi} \displaystyle\int_0^{\pi} \left[\int_0^{2\pi} \begin{pmatrix} \delta_{ik} n_j n_l + \delta_{jk} n_i n_l + \\ \delta_{il} n_k n_j + \delta_{jl} n_k n_i \end{pmatrix} \mathbf{n}^{-1} d\theta \right] \sin\phi d\phi \\ Q_{ijkl} = \dfrac{3}{4\pi} \displaystyle\int_0^{\pi} \left[\int_0^{2\pi} \left(n_i n_j n_k n_l \right) \mathbf{n}^{-3} d\theta \right] \sin\phi d\phi \\ \mathbf{n} = \sqrt{n_i n_i} \\ n = \left(\dfrac{\sin\phi\cos\theta}{a_1}; \dfrac{\sin\phi\sin\theta}{a_2}; \dfrac{\cos\phi}{a_3} \right)^{\mathrm{T}} \end{cases} \tag{35}$$

REFERENCES

[1] Kuilla, T., Bhadra, S., Yao, D., Kim, N. H., Bose, S., and Lee, J. H., 2010. "Recent advances in graphene based polymer composites". *Progress in Polymer Science,* ***35***(11), pp. 1350 – 1375.

[2] Xiao, J., Gama, B., and Jr., J. G., 2005. "An analytical molecular structural mechanics model for the mechanical properties of carbon nanotubes". *International Journal of Solids and Structures,* ***42***, pp. 3075 – 3092.

[3] Cho, J., Luo, J., and Daniel, I., 2007. "Mechanical characterization of graphite/epoxy nanocomposites by multi-scale analysis". *Composites Science and Technology,* ***67***(1112), pp. 2399 – 2407.

[4] Rafiee, M. A., Rafiee, J., Srivastava, I., Wang, Z., Song, H., Yu, Z.-Z., and Koratkar, N., 2010. "Fracture and fatigue in graphene nanocomposites". *Small,* ***6***(2), pp. 179–183.

[5] Veca, L. M., Meziani, M. J., Wang, W., Wang, X., Lu, F., Zhang, P., Lin, Y., Fee, R., Connell, J. W., and Sun, Y.-P., 2009. "Carbon nanosheets for polymeric nanocomposites with high thermal conductivity". *Advanced Materials,* ***21***(20), pp. 2088–2092.

[6] Xu, Z., and Gao, C., 2010. "In situ polymerization approach to graphene-reinforced nylon-6 composites". *Macromolecules,* ***43***(16), pp. 6716–6723.

[7] Zhang, W. L., Park, B. J., and Choi, H. J., 2010. "Colloidal graphene oxide/polyaniline nanocomposite and its electrorheology". *Chem. Commun.,* ***46***, pp. 5596–5598.

[8] Yanase, K., and Ju, J., 2014. "Overall elastoplastic damage responses of spherical particle-reinforced composites containing imperfect interfaces". *International Journal of Damage Mechanics,* ***vol. 23***(no. 3), pp. 411–429.

[9] Walpole, L.-J., 1978. "A coated inclusion in an elastic medium". *Mathematical Proceedings of the Cambridge Philosophical Society,* ***83***, p. 495.

[10] Christensen, R. M., and Lo, K. H., 1979. "Solutions for effective shear properties in three phase sphere and cylinder models". *Journal of the Mechanics and Physics of Solids,* ***27***(4), pp. 315 – 330.

[11] Hervé, E., and Zaoui, A., 1993. "n-layered inclusion-based micromechanical modelling". *International Journal of Engineering Science,* ***31***(1), pp. 1 – 10.

[12] Cherkaoui, M., Sabar, H., and Berveiller, M., 1994. Micromechanical approach of the coated inclusion problem and applications to composite materials. Journal of engineering materials and technology. vol. 116, no 3 (11 ref.), pp. 274-278.

[13] Lipinski, P., Barhdadi, E., and Cherkaoui, M., 2006. "Micromechanical modeling of an arbitrary ellipsoidal multi-coated inclusion". *Philosophical Magazine,* ***86***(10), pp. 1305–1326.

[14] Matous, K., and Geubelle, P. H., 2006. "Finite element formulation for modeling particle debonding in reinforced elastomers subjected to finite deformations". *Computer Methods in Applied Mechanics and Engineering,* ***196***(1-3), pp. 620 – 633.

[15] Inglis, H., Geubelle, P., MatouÅ¡, K., Tan, H., and Huang, Y., 2007. "Cohesive modeling of dewetting in particulate composites: micromechanics vs. multiscale finite element analysis". *Mechanics of Materials,* ***39***(6), pp. 580 – 595.

[16] Tan, H., Huang, Y., Liu, C., and Geubelle, P., 2005. "The mori-tanaka method for composite materials with nonlinear interface debonding". *International Journal of Plasticity,* ***21***(10), pp. 1890 – 1918.

[17] Tan, H., Liu, C., Huang, Y., and Geubelle, P., 2005. "The cohesive law for the particle/matrix interfaces in high explosives". *Journal of the Mechanics and Physics of Solids,* ***53***(8), pp. 1892 – 1917.

Copyright © 2016 by ASME

[18] Ghahremani, F., 1980. "Effect of grain boundary sliding on anelasticity of polycrystals". *International Journal of Solids and Structures,* ***16***(9), pp. 825 – 845.

[19] Sharma, P., Ganti, S., and Bhate, N., 2003. "Effect of surfaces on the size-dependent elastic state of nano-inhomogeneities". *Appl. Phys. Lett,* ***82***, p. 535.

[20] Sharma, P., and Ganti, S., 2004. Size-dependent eshelby's tensor for embedded nano-lnclusions incorporating surface/interface energies. Journal of applied mechanics.

[21] Sharma, P., and Wheeler, L. T., 2007. "Size-dependent elastic state of ellipsoidal nano-inclusions incorporating surface/interface tension". *Journal of Applied Mechanics,* ***Vol. 74***, p. 447.

[22] Duan, H., Wang, J., Huang, Z., and Karihaloo, B., 2005. "Eshelby formalism for nano-inhomogeneities". *Proc. R. Soc. A,* ***461***, pp. 3335–3353.

[23] Duan, H., Wang, J., Huang, Z., and Karihaloo, B., 2005. "Size-dependent effective elastic constants of solids containing nano-inhomogeneities with interface stress". *Journal of the Mechanics and Physics of Solids,* ***53***(7), pp. 1574 – 1596.

[24] Hashin, Z., 1991. "The spherical inclusion with imperfect interface". *Journal of Applied Mechanics,* ***58***(2), June, pp. 444–449.

[25] Hashin, Z., 1991. "Thermoelastic properties of particulate composites with imperfect interface". *Journal of the Mechanics and Physics of Solids,* ***39***(6), pp. 745 – 762.

[26] Qu, J., 1993. "The effect of slightly weakened interfaces on the overall elastic properties of composite materials". *Mechanics of Materials,* ***14***(4), pp. 269 – 281.

[27] Qu, J., 1993. "Eshelby tensor for an elastic inclusion with slightly weakened interface". *Journal of Applied Mechanics,* ***60***(4), Dec., pp. 1048–1050.

[28] Zhong, Z., and Meguid, S. A., 1997. "On the elastic field of a shpherical inhomogeneity with an imperfectly bonded interface". *Journal of Elasticity,* ***46***(2), pp. 91–113.

[29] Yu, H., 1998. "A new dislocation-like model for imperfect interfaces and their effect on load transfer". *Composites Part A: Applied Science and Manufacturing,* ***29***(9-10), pp. 1057 – 1062.

[30] Yu, H., Wei, Y., and Chiang, F., 2002. "Load transfer at imperfect interfaces-dislocation-like model". *International Journal of Engineering Science,* ***40***(14), pp. 1647 – 1662.

[31] Zhao, Y., and Weng, G., 1997. "Transversely isotropic moduli of two partially debonded composites". *International Journal of Solids and Structures,* ***34***(4), pp. 493 – 507.

[32] Zhao, Y. H., and Weng, G. J., 2002. "The effect of debonding angle on the reduction of effective moduli of particle and fiber-reinforced composites". *Journal of Applied Mechanics,* ***69***(3), May, pp. 292–302.

[33] Dederichs, P. H., and Zeller, R., 1973. "Variational treatment of the elastic constants of disordered materials". *Zeitschrift für Physik A Hadrons and Nuclei,* ***259***(2), pp. 103–116.

[34] Azoti, W., Koutsawa, Y., Tchalla, A., Makradi, A., and Belouettar, S., 2015. "Micromechanics-based multi-site modeling of elastoplastic behavior of composite materials". *International Journal of Solids and Structures,* ***59***, pp. 198 – 207.

[35] Azoti, W., Tchalla, A., Koutsawa, Y., Makradi, A., Rauchs, G., Belouettar, S., and Zahrouni, H., 2013. "Mean-field constitutive modeling of elasto-plastic composites using two (2) incremental formulations". *Composite Structures,* ***105***, pp. 256–262.

[36] Doghri, I., and Ouaar, A., 2003. "Homogenization of two-phase elasto-plastic composite materials and structures: Study of tangent operators, cyclic plasticity and numerical algorithms". *International Journal of Solids and Structures,* ***40***(7), pp. 1681 – 1712.

[37] Vieville, P., Bonnet, A. S., and Lipinski, P., 2006. "Modelling effective properties of composite materials using the inclusion concept. general considerations". *Arch. Mech.,* ***58***(3), pp. 207–239.

[38] Fassi-Fehri, O., 1985. "Le probleme de la paire d'inclusions plastiques et heterogenes dans une matrice anisotrope : Application a l'etude du comportement des materiaux composites et de la plasticite". PhD thesis, Universite de Metz.

[39] Eshelby, J. D., 1957. "The determination of the elastic field of an ellipsoidal inclusion, and related problems". *Proceedings of the Royal Society of London. Series A, Mathematical and Physical Sciences,* ***241***(1226), pp. 376–396.

Copyright © 2016 by ASME